

Modulation of the mechanism of apoptosis in cancer cell lines by treatment with silica-based nanostructured materials functionalized with different metallodrugs.

Diana Díaz-García^a, Diana Cenariu^b, Yolanda Pérez^a, Paula Cruz^a, Isabel del Hierro^a, Sanjiv Prashar^a, Eva Fischer-Fodor^{b,c,*} and Santiago Gómez-Ruiz^{a,*}

^a Departamento de Biología y Geología, Física y Química Inorgánica, ESCET, Universidad Rey Juan Carlos, Calle Tulipán s/n, E-28933, Móstoles (Madrid), Spain

^b Medfuture - Research Center for Advanced Medicine, The University of Medicine and Pharmacy "Iuliu Hatieganu", RO-400337, Cluj-Napoca, Romania.

^c Tumour Biology Department, The Institute of Oncology "I.Chiricuta", RO-400015, Cluj-Napoca, Romania.

† *Corresponding authors: S. Gómez-Ruiz, e-mail address: santiago.gomez@urjc.es and E. Fischer-Fodor, e-mail address: fischer.eva@iocn.ro

Supplementary Material

This supplementary material contains: Pore size distribution of SBA-PADOH and **M1–M3**, FT-IR spectra of SBA-PADOH and **M1–M3**, DR-UV spectra of SBA-PADOH and **M1–M3**, particle size distribution of SBA-PADOH and **M1–M3** and additional biological data.

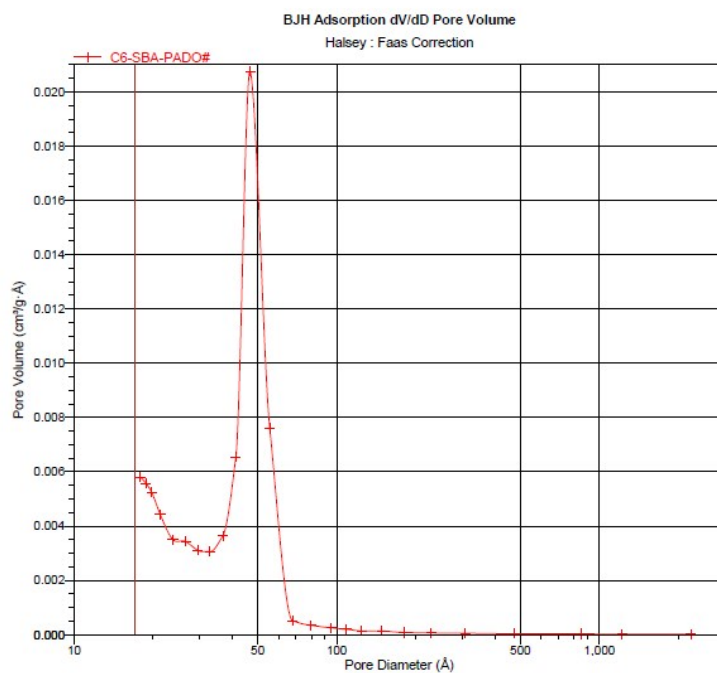


Figure S1. Pore size distribution of SBA-PADOH

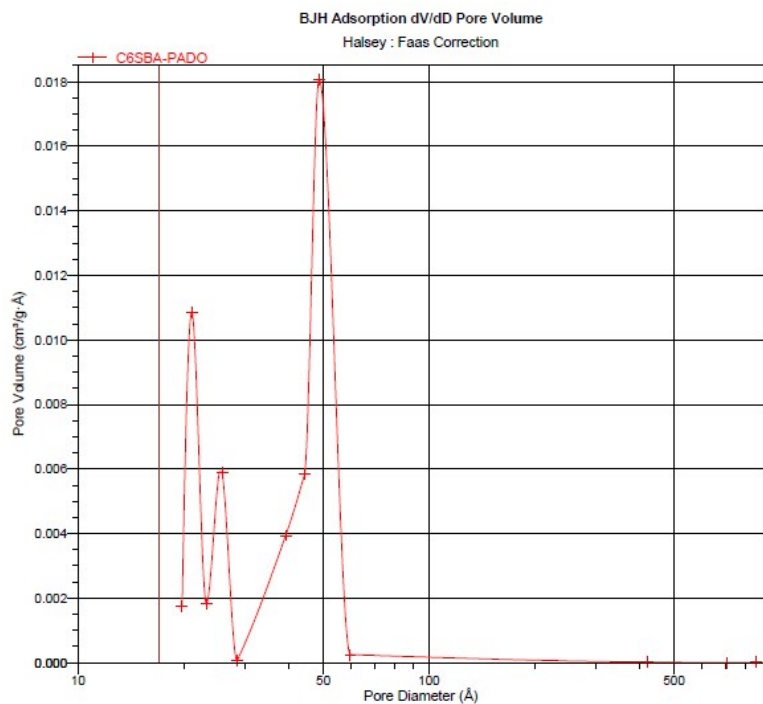


Figure S2. Pore size distribution of **M1**

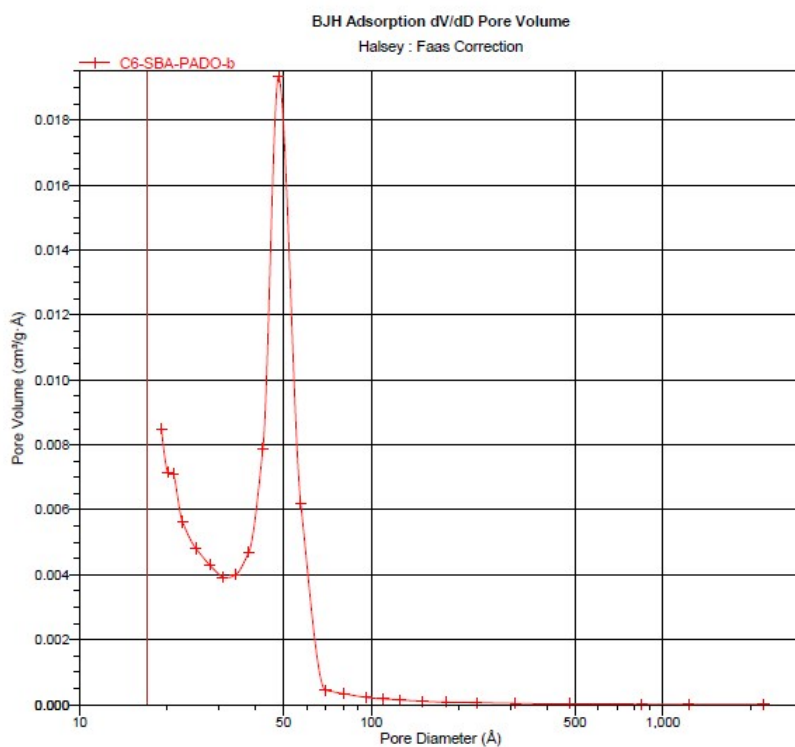


Figure S3. Pore size distribution of **M2**

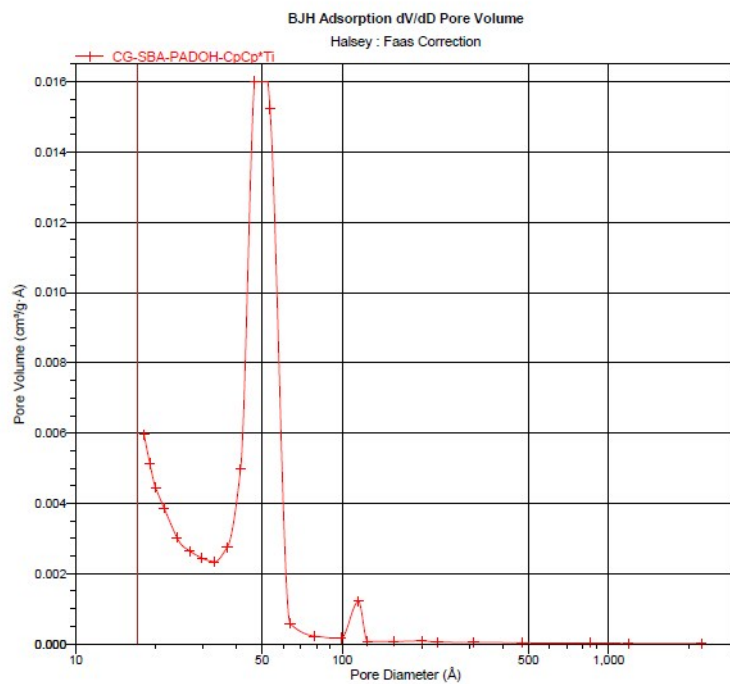


Figure S4. Pore size distribution of M3

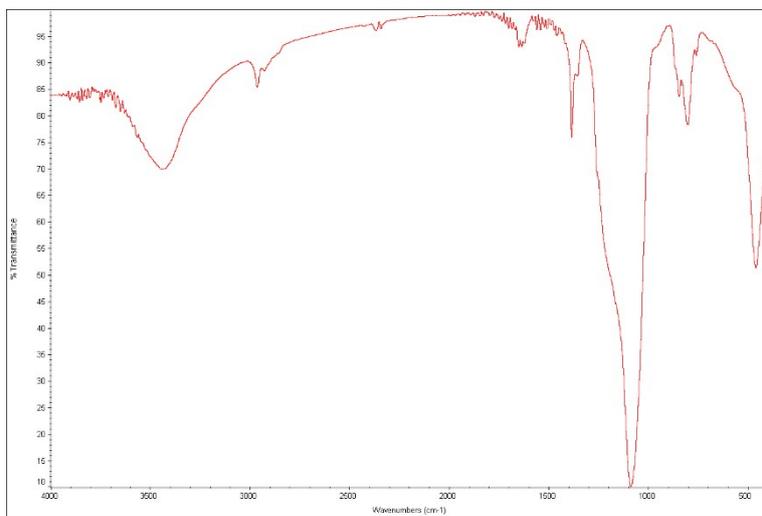


Figure S5. FT-IR spectrum of SBA-PADOH

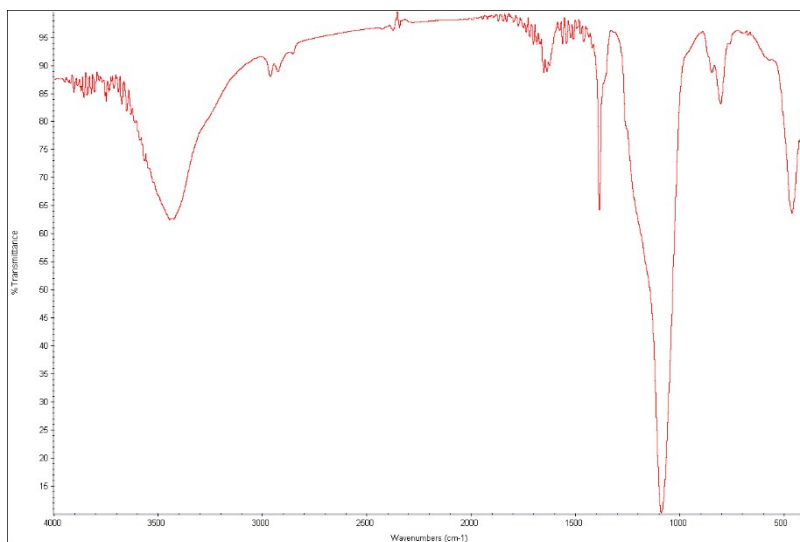


Figure S6. FT-IR spectrum of **M1**

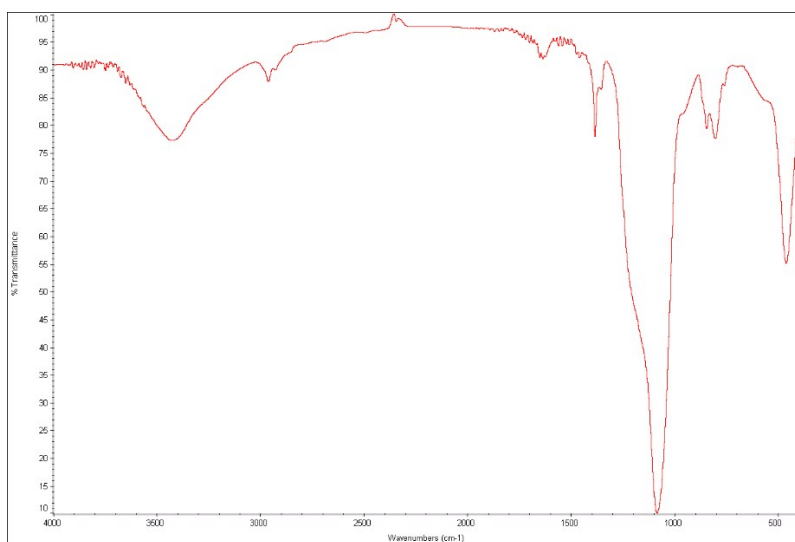


Figure S7. FT-IR spectrum of **M2**

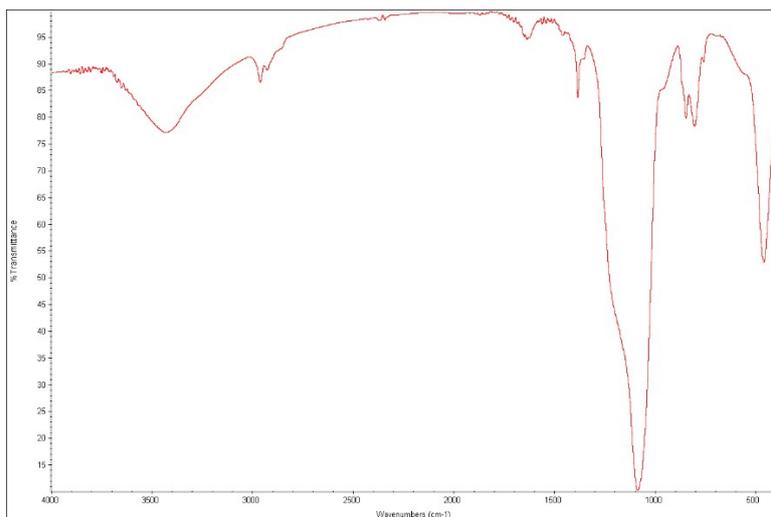


Figure S8. FT-IR spectrum of **M3**

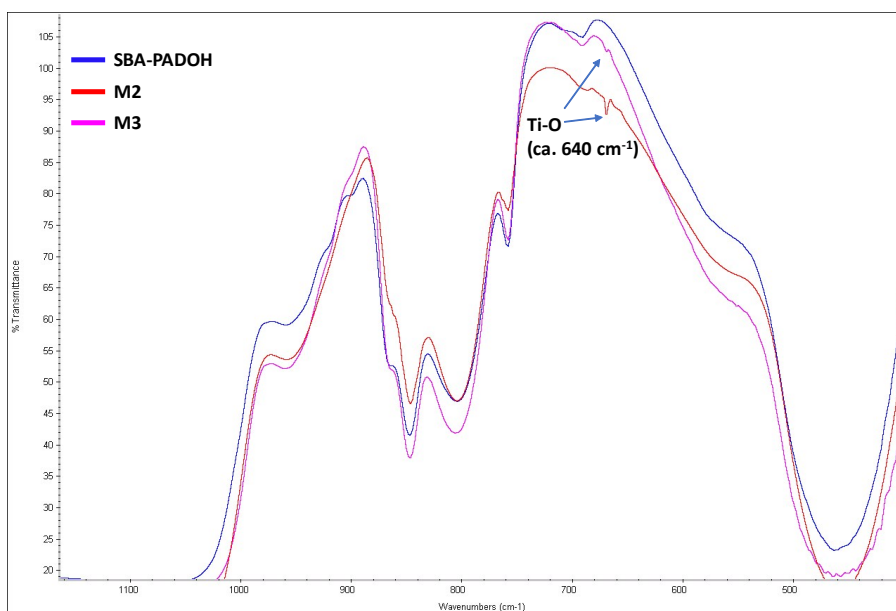


Figure S9. Comparison of FT-IR spectra of SBA-PADOH, **M2** and **M3** for the detection of Ti-O band.

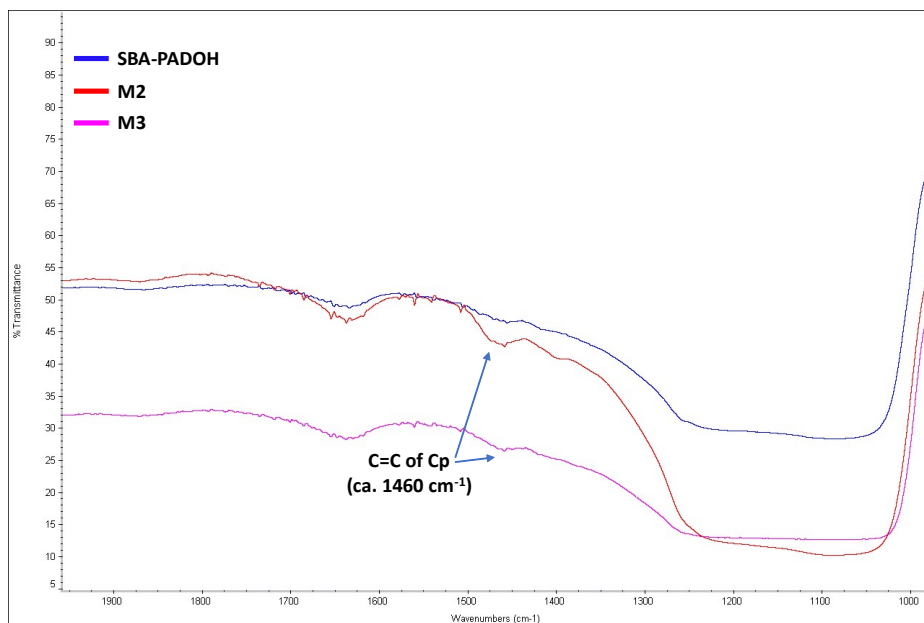


Figure S10. Comparison of FT-IR spectra of SBA-PADOH, **M2** and **M3** for the detection of C=C band of Cp ligands.

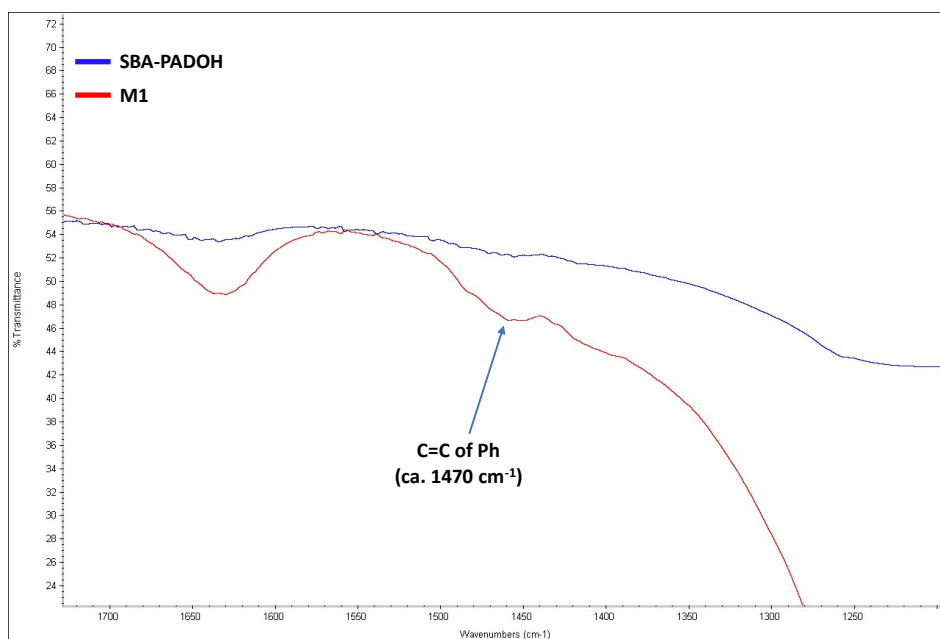


Figure S11. Comparison of FT-IR spectra of SBA-PADOH and **M1** for the detection of C=C band of Ph ligands.

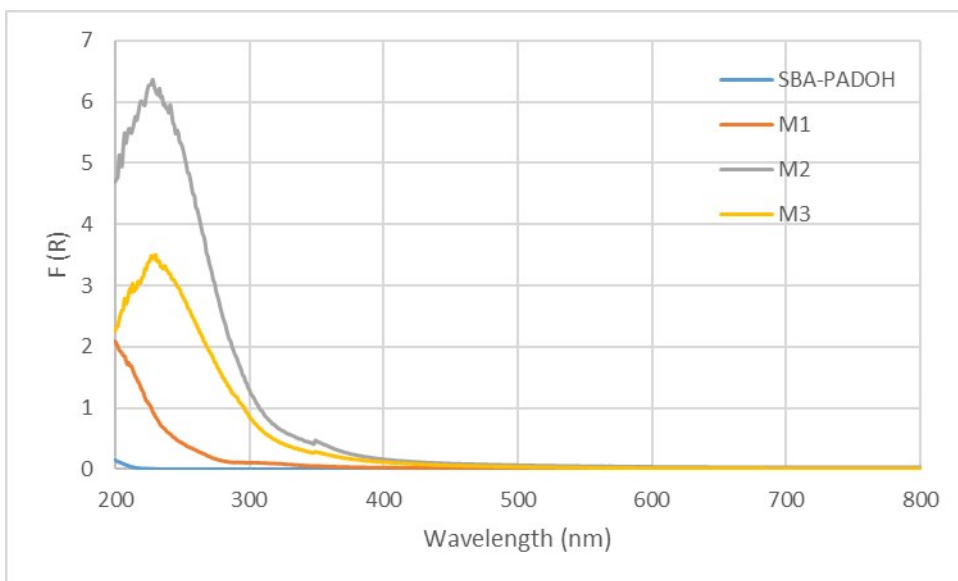


Figure S12. DR-UV spectra of SBA-PADOH, M1, M2 and M3.

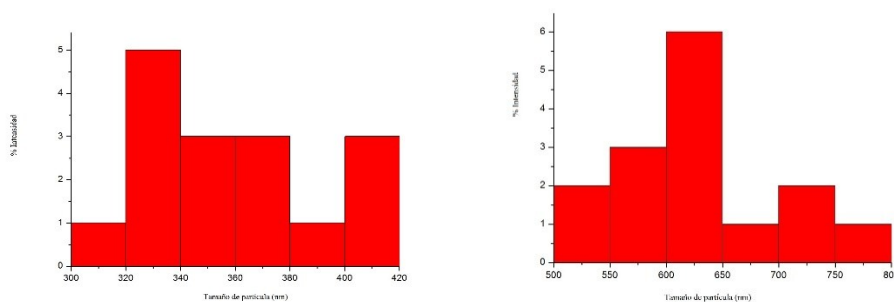


Figure S13. Particle size distribution of SBA-PADOH (x axis size in nm, y axis number of particles). Left: distribution of particle width; right: distribution of particle length.

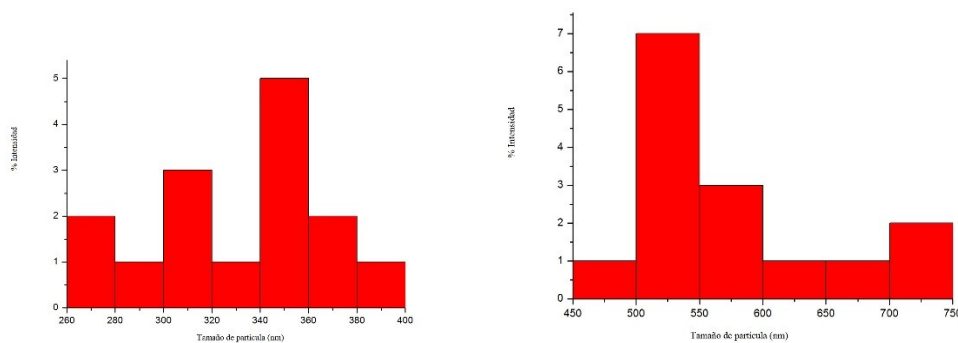


Figure S14. Particle size distribution of M1(x axis size in nm, y axis number of particles). Left: distribution of particle width; right: distribution of particle length.

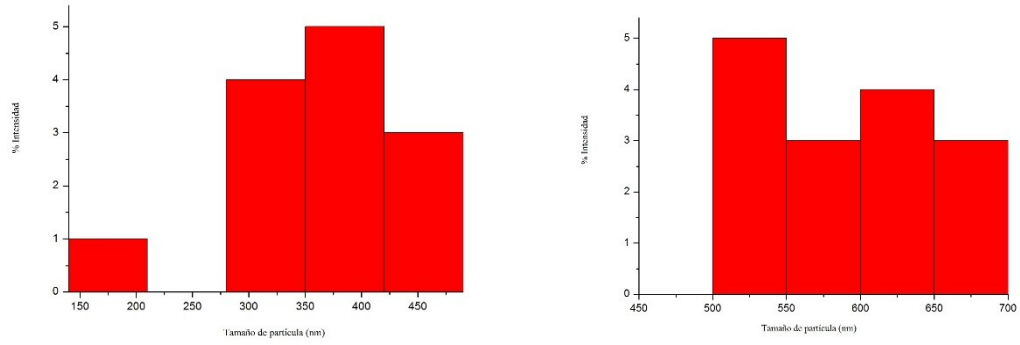


Figure S15. Particle size distribution of **M2**(x axis size in nm, y axis number of particles). Left: distribution of particle width; right: distribution of particle length.

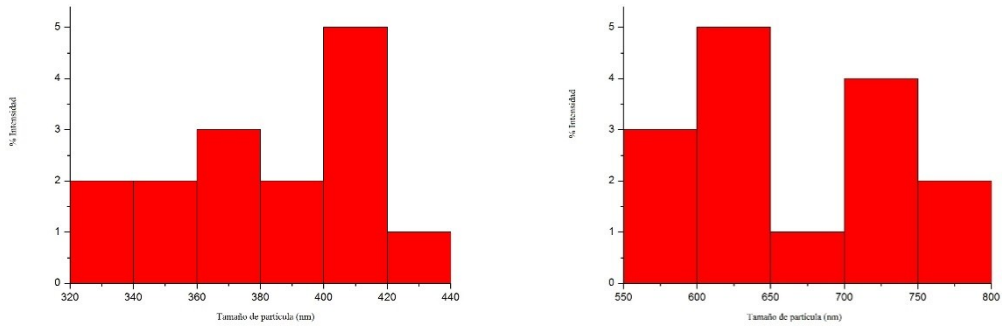


Figure S16. Particle size distribution of **M3**(x axis size in nm, y axis number of particles). Left: distribution of particle width; right: distribution of particle length.

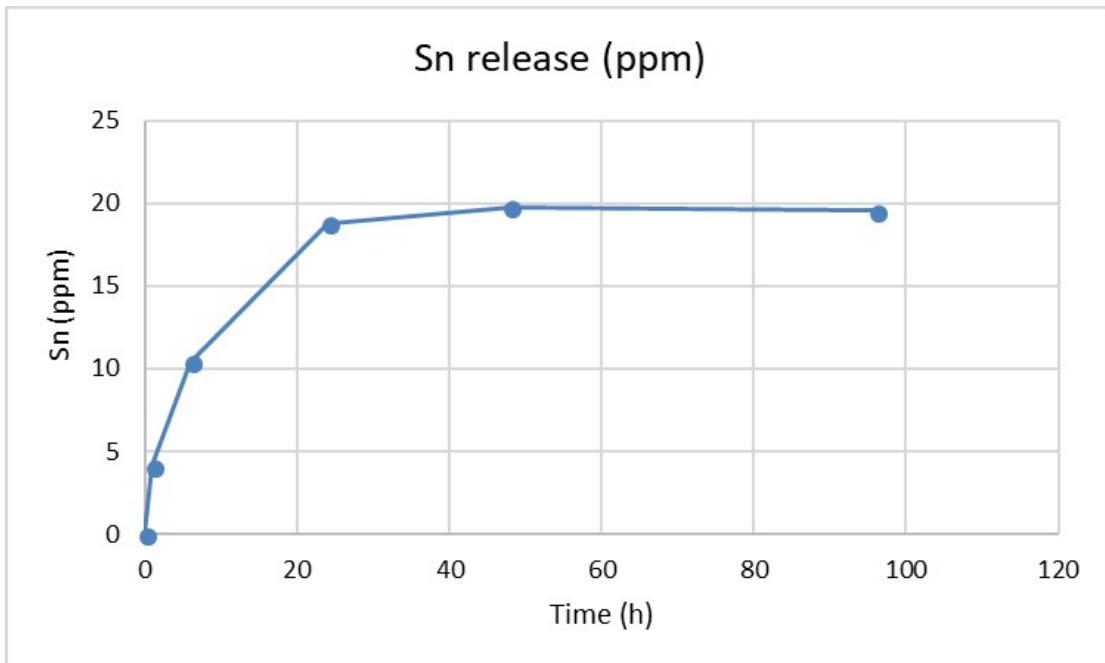


Figure S17.Release study of material **M1** in simulated body fluid (ppm of Sn released to the medium)

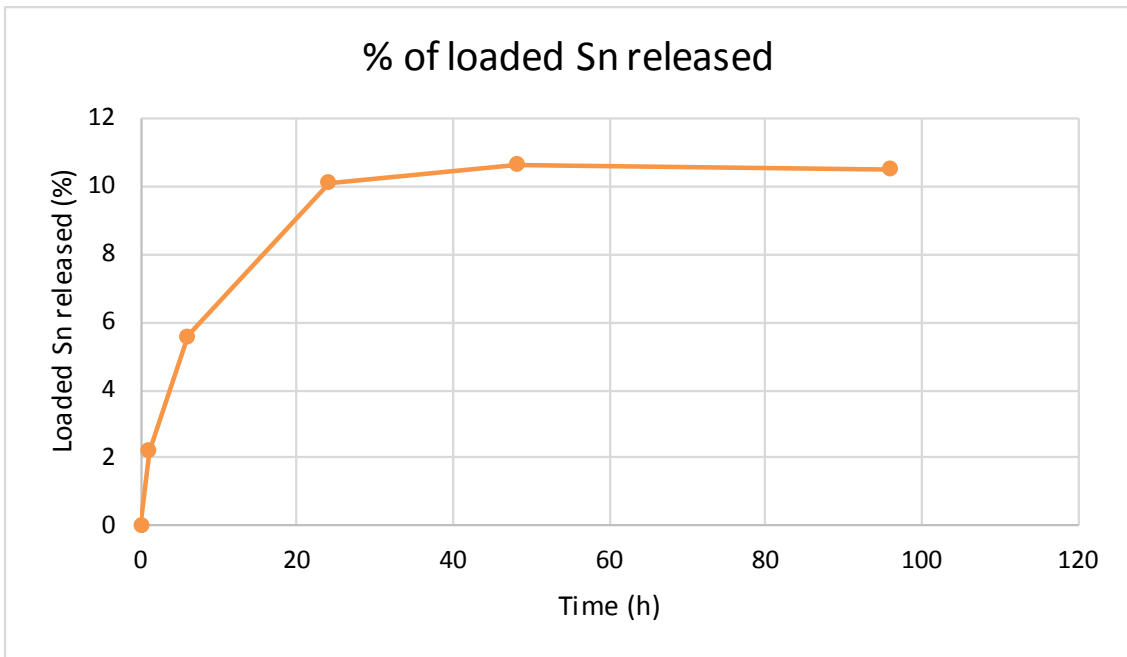


Figure S18.Release study of material **M1** in simulated body fluid (% of loaded Sn released to the medium)

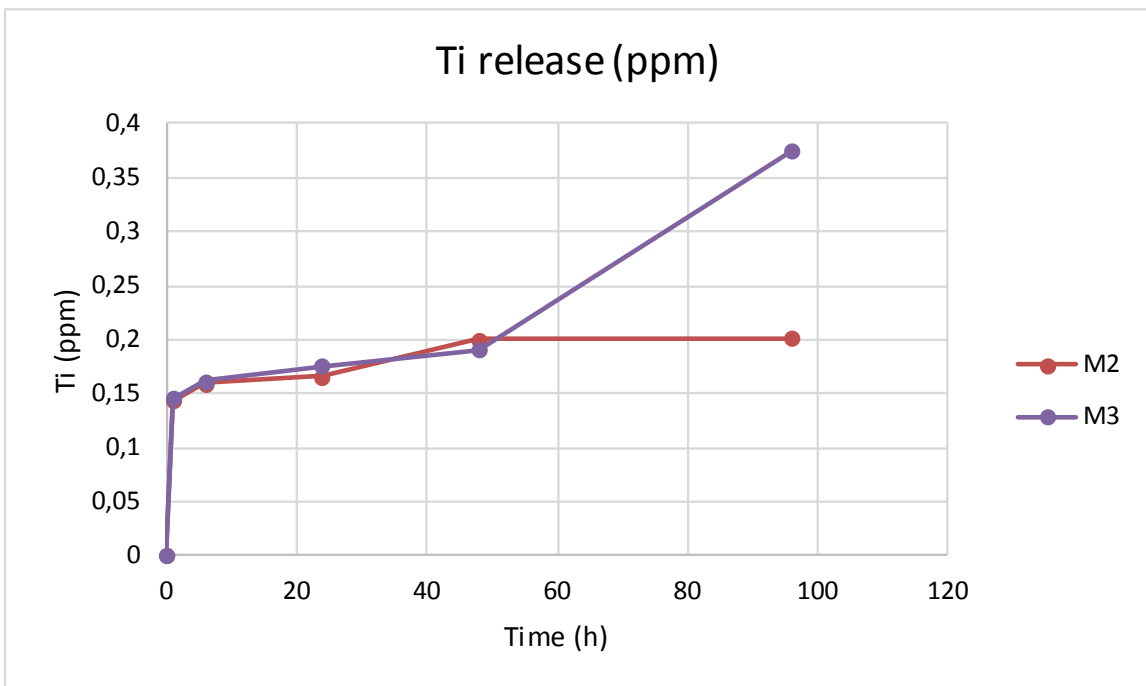


Figure S19.Release study of material **M2** and **M3** in simulated body fluid (ppm of Ti released to the medium)

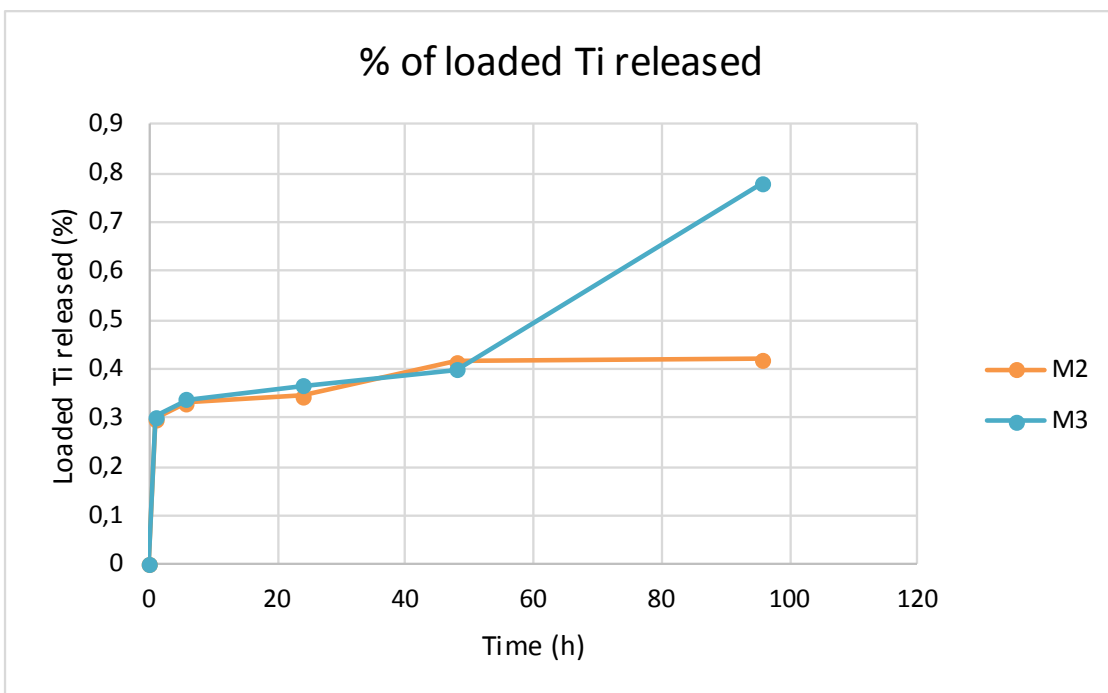


Figure S20. Release study of material **M2** and **M3** in simulated body fluid (% of loaded Ti released to the medium)

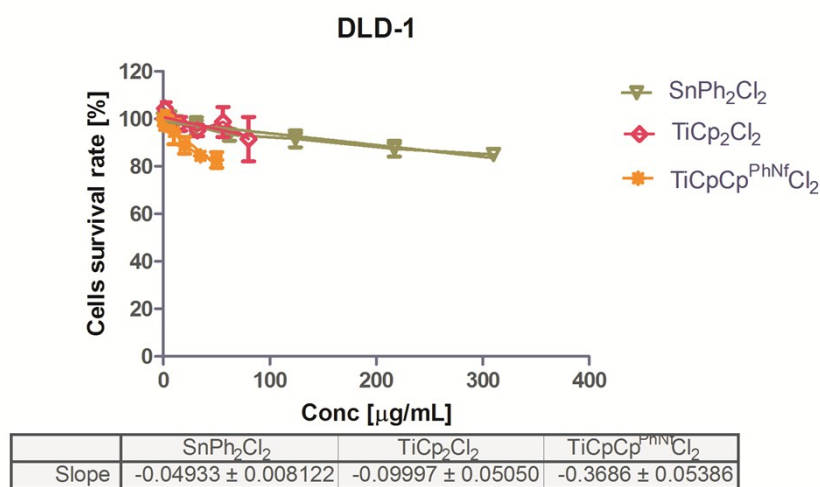
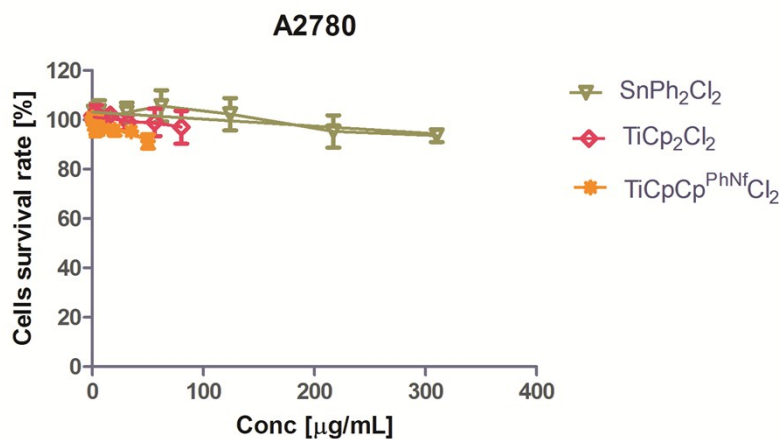
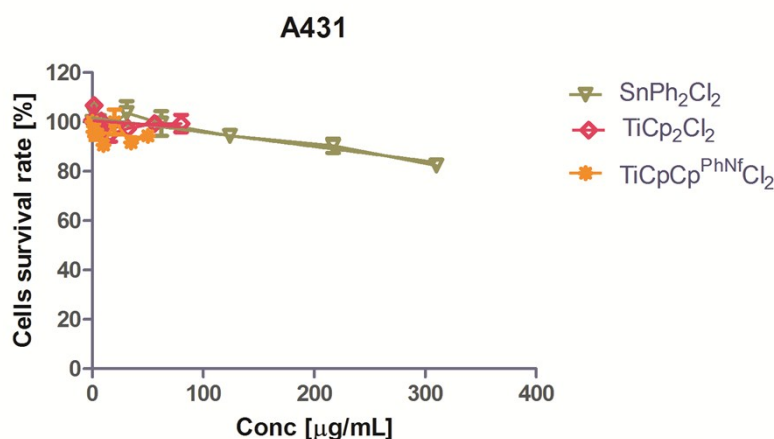


Figure S21. Reduction of the metabolic rate in DLD-1 colon carcinoma cells after the treatment with SnPh₂Cl₂, the active compound incorporated in **M1**; TiCp₂Cl₂, the precursor of **M2** and TiCpCp^{PhNf}Cl₂, precursor of **M3**. The linear regression of the fluorescence data measured after 24 hours of incubation indicates a slight, but statistically significant, decrease ($p < 0.05$) of the metabolic rate for SnPh₂Cl₂ and TiCpCp^{PhNf}Cl₂, while TiCp₂Cl₂ has no significant activity. In SnPh₂Cl₂ the metabolic rate maintains over 85% for every applied concentration, while in TiCpCp^{PhNf}Cl₂ this percent is 82.7%.



	SnPh ₂ Cl ₂	TiCp ₂ Cl ₂	TiCpCp ^{PhNf} Cl ₂
Slope	-0.02846 ± 0.01331	-0.04775 ± 0.03709	-0.1441 ± 0.03806

Figure S22. Metabolic rate reduction in A2780 ovary carcinoma cells treated with with SnPh₂Cl₂, TiCp₂Cl₂, and TiCpCp^{PhNf}Cl₂ alone, without incorporation into **M1-M3**. The linear regression of data indicates significant activity in SnPh₂Cl₂ and TiCpCp^{PhNf}Cl₂. The metabolic rate maintains over 91% even using the highest concentration.



	SnPh ₂ Cl ₂	TiCp ₂ Cl ₂	TiCpCp ^{PhNf} Cl ₂
Slope	-0.05810 ± 0.009082	-0.03165 ± 0.02821	-0.06006 ± 0.05756

Figure S23. Metabolic rate reduction in A431 epidermal carcinoma cells treated with with SnPh₂Cl₂, TiCp₂Cl₂, and TiCpCp^{PhNf}Cl₂ alone, without incorporation into **M1-M3**. The metabolic rate reduction was significant only for SnPh₂Cl₂, where the 82.3 percent of the cells were still metabolically active after the treatment.

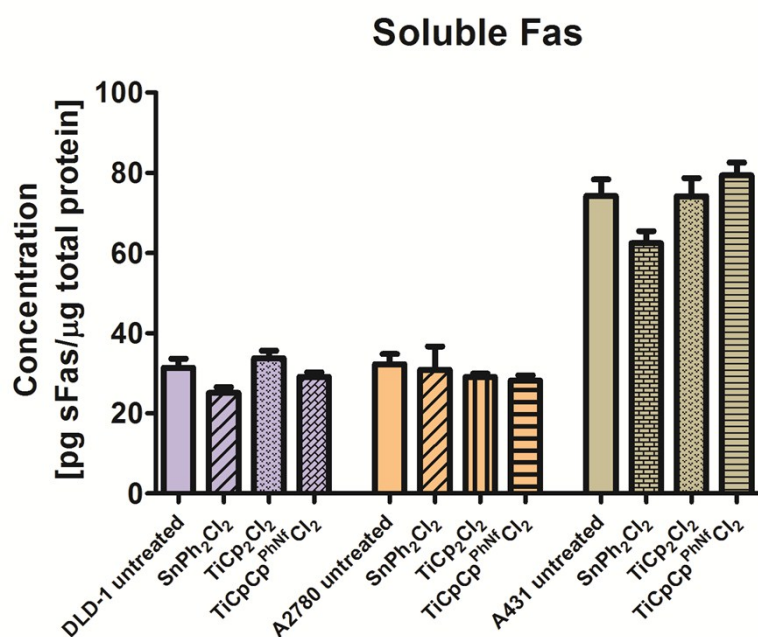


Figure S24. Influence of SnPh₂Cl₂, TiCp₂Cl₂, and TiCpCp^{PhNf}Cl₂ on the level of soluble Fas receptor secreted by DLD-1, A2780 and A431 tumor cells. The same concentration of compounds alone, without being incorporated in SBA-PADOH, does not exhibit any statistically significant influence on Fas receptor (one-way analysis of variances, p<0.05).

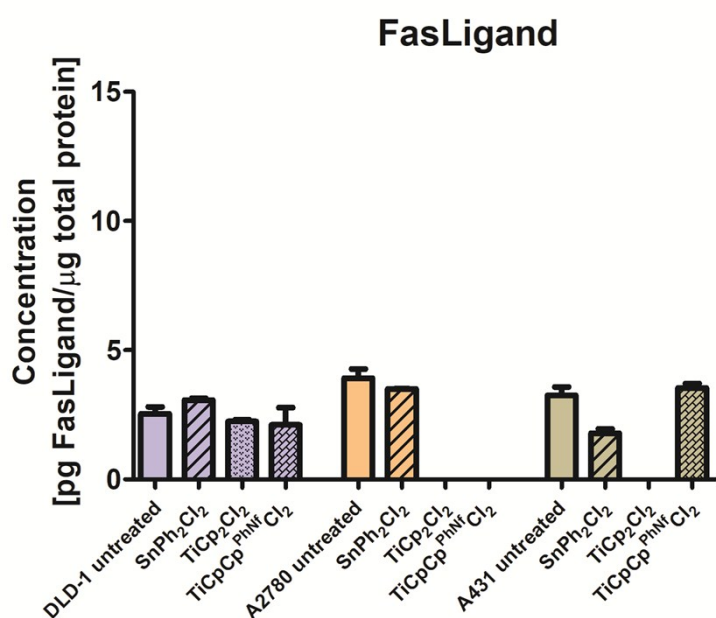


Figure S25. Influence of SnPh₂Cl₂, TiCp₂Cl₂, and TiCpCp^{PhNf}Cl₂ on the level of Fas Ligand secreted by DLD-1, A2780 and A431 tumor cells; the protein level was below the detection limit in three samples, and no significant modulation was evidenced using the one-way analysis of variances.

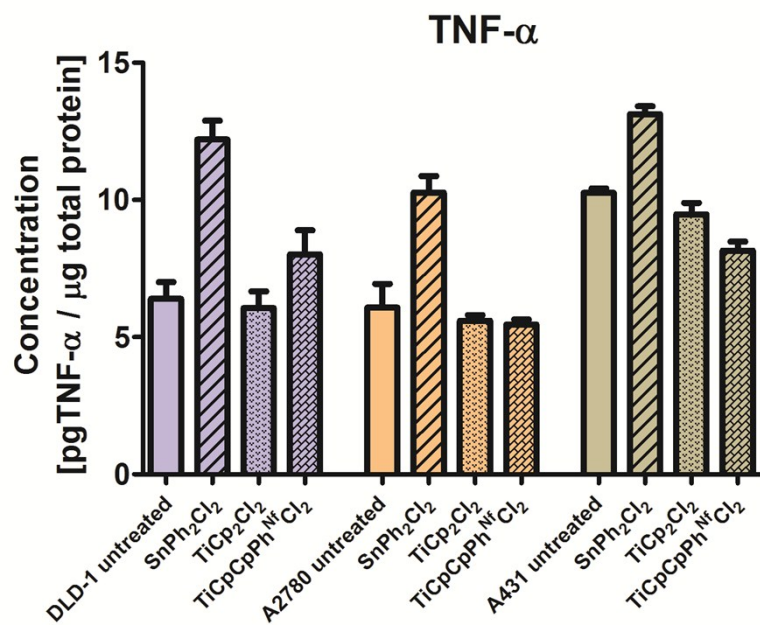


Figure S26. Influence of SnPh₂Cl₂, TiCp₂Cl₂, and TiCpCp^{PhNf}Cl₂ on the tumor necrosis factor alpha (TNF-α) secreted by DLD-1, A2780 and A431 tumor cells. SnPh₂Cl₂, the precursor of **M1** caused a significant increase of TNF-α production (one-way analysis of variance, p<0.05), while the titanocenes exhibited no significant influence in the tumour cell lines.

Table S1. Particle size distribution of SBA-PADOH and **M1–M3**.

	Width (nm)	Length (nm)
SBA-PADOH	339±10	603±24
M1	357±10	546±24
M2	377±54	549±17
M3	407±8	604±25